Syntectonic fluid-rock interaction and mineral reactions in amphibolites from the Adula nappe (Central Alps, Switzerland)

by *Michael Dalla Torre*[1,2] and *Julius H. Partzsch*[1,3]

Abstract

Mineral reactions and fluid flux calculations from the basal part of the Adula nappe and the upper part of the Simano nappe (Central Alps, Switzerland) are presented. The base of the Adula nappe (hangingwall) and the upper part of the Simano nappe (footwall) contain a series of amphibolite layers that are coherently intercalated with gneisses. The intercalations are subparallel to the metacarbonates of the Soja zone, which separates the two nappes. Our data indicate that during emplacement of the Adula onto the Simano nappe and its autochthonous cover, the Soja zone, amphibolite layers were altered by a mixed CO_2–H_2O fluid. However, the alteration is restricted to amphibolites that are adjacent to the metacarbonates. Amphibolites located further away from the Soja zone do not show any alteration by a mixed CO_2–H_2O fluid. Field data indicate that the fluid apparently was released from the metacarbonates of the Soja zone. Compositional variations in amphibole from amphibolites from the basal part of the Adula nappe indicate that the process of fluid infiltration and associated mineral reactions occurred during progressive metamorphism from greenschist to epidote-amphibolite facies conditions. Two distinct mineral reactions were observed. (i) Amphibolite layers located close to the metacarbonates adjusted their mineral assemblages and the compositions of their minerals toward an equilibrium with the infiltrating fluid. These rocks experienced carbonation-dehydration reactions. (ii) Amphibolite layers located about 40 m above the basal thrust of the Adula nappe did not react with CO_2 and experienced hydration reactions only. The differences in mineral reaction from one amphibolite layer to another suggest that the first layers on either side of the metacarbonates retained CO_2 from the fluid phase. Thus, the fluid that left this layer was depleted in CO_2. Thermodynamic computations of phase equilibria in temperature-X_{CO_2} sections at isobaric conditions (7 kbar) suggest that X_{CO_2} in equilibrium with the rock was at about 0.05 ± 0.03. This value is equal to the mole fraction of CO_2 of the infiltrating fluid. Fluid flux calculations indicate that the basal amphibolite layers were infiltrated by variable amounts of fluid ranging from 47 to 158 cm^3 (fluid)/cm^2 (rock).

Keywords: fluid-rock interaction, exchange vector, net transfer reaction, metamorphism, amphibolite, Adula nappe, Central Alps, Switzerland.

Introduction

Theoretical considerations on fluid flux in ancient hydrothermal systems have been presented by several researchers (e.g., KORZHINSKII, 1970; FRANTZ and WEISBROD, 1974; BAUMGARTNER and FERRY, 1991; FERRY and DIPPLE, 1991). KORZHINSKII (1970) and FRANTZ and WEISBROD (1974), for example, used mass conservation considerations to describe quantitatively changes in the mineralogical composition of a rock that was affected by an infiltrating fluid. The equations presented by these authors allow to estimate the progress of a reaction front proceeding in a rock. A different approach was used by BAUMGARTNER and FERRY (1991) and FERRY and DIPPLE (1991). Based on the theory of fluid flow through porous media, these authors provided an equation that relates reaction progress to the amount of fluid in equilibrium with the rock. The main difference between the two models is due to the fact that the latter requires the fluid composition to be

[1] Mineralogisch-Petrographisches Institut, Universität Basel, Bernoullistrasse 30, CH-4056 Basel, Switzerland.
[2] Present address: Department of Environmental Geological Sciences, Stanford University, Stanford, CA 94305-2115, USA. E-mail: mica@pangea.stanford.edu.
[3] Present address: Universität Potsdam, Institut für Geowissenschaften, Mineralogie-Petrologie, Postfach 601553, D-14415 Potsdam, Deutschland.

buffered by the composition of the rock along its flow path. However, this condition is not required if the model by KORZHINSKII (1970) and FRANTZ and WEISBROD (1974) is applied. RICE and FERRY (1982) called the process of buffering of the fluid composition by the mineral assemblage "internal buffering".

Reactions between a fluid and a rock may occur under different conditions. If the infiltrating fluid is not in equilibrium with the rock, reaction fronts develop separating the unaltered protolith from the altered rock. Under equilibrium conditions between fluid and rock, reactions occur if there is a temperature or pressure gradient along the flow path (FERRY, 1991). The amount of phases produced and consumed during the reaction is a measure of the progress of the reaction (e.g., FRANTZ and WEISBROD, 1974; RICE and FERRY, 1982). In recent studies, fluid fluxes for areas affected by regional and contact metamorphism were calculated (e.g., RICE and FERRY, 1982; FERRY and DIPPLE, 1991; FERRY, 1991; BAUMGARTNER and FERRY, 1991; LÉGER and FERRY, 1993; FERRY, 1995). According to these results, metamorphism driven by fluid infiltration requires variable fluid fluxes. FERRY and DIPPLE (1991) concluded that CO_2 metasomatism (e.g., carbonation or decarbonation reactions) requires high fluxes on the order of 10^4–10^6 cm^3/cm^2, whereas H_2O metasomatism (e.g., hydration or dehydration reactions) requires lower values (10^2–10^4 cm^3/cm^2). Very high fluid fluxes were calculated for the process of major element metasomatism (10^6–10^8 cm^3/cm^2), or the formation of quartz veins (10^8–10^9 cm^3/cm^2). These values were calculated using the approach by FERRY and DIPPLE (1991) and BAUMGARTNER and FERRY (1991).

In this study, we present data on fluid-rock interaction at the base of the Adula nappe and the top of the Simano nappe (Central Alps, Switzerland). Amphibolites from both the Adula and the Simano nappes show evidence of infiltration of a mixed CO_2–H_2O fluid. The infiltration features are limited to amphibolite layers that are close (< 20 m) to the metacarbonates of the Soja zone. This unit represents the former autochthonous cover of the Simano nappe and separates this unit from the Adula nappe. Amphibolites located further away from either side of the contacts do not show any alteration by a fluid. The goal of this study is to constrain the initial fluid composition, as well as to document the difference in mineral reaction between samples infiltrated by a mixed CO_2–H_2O fluid and those that did not react with CO_2.

ABBREVIATIONS OF ENDMEMBER PHASES AND EXCHANGE VECTORS

am = amphibole; an = anorthite; bt = biotite; cal = calcite; czo = clinozoisite; grs = grossular; grt = garnet; ilm = ilmenite; ms = muscovite; phl = phlogopite; plag = plagioclase; qtz = quartz; rt = rutile; ttn = titanite; tr = tremolite; tsch = tschermakite; zo = zoisite; FM = $FeMg_{-1}$; ferri = $Fe^{+3}Al_{-1}$; ed = $NaAlSi_{-1}$; pa = NaK_{-1}; pl = $NaSiCa_{-1}Al_{-1}$; ts = $Al_2Si_{-1}Mg_{-1}$; exti = $TiMgAl_{-2}$.

Methods

All samples were investigated by optical microscopy. Electron microprobe analysis (EMP) was performed for two samples using wavelength-dispersive spectroscopy (WDS) on a JEOL JXA-8600 Superprobe with Voyager automation at Basel University. Silicate standards were used for silicates. For calcite, carbonate standards were used. The operating conditions included an accelerating voltage of 15 kV, a beam current of 10 nA, and an acquisition time of 60 seconds or until 0.4% precision on the counting statistics was obtained. The data were reduced using a ZAF correction program.

Modal abundances of minerals were determined in two different ways: (i) using a point counter and a step size of 300 μm, by counting 2000 points per thin section, (ii) mineral grain boundaries were retraced from thin sections with a petroscope. The resulting image was digitized, and the total area of each mineral was measured using the computer program IMAGE (RASBAND, 1993).

Major and trace elements of the investigated samples were analyzed on polished surfaces (ca. 1 cm^2) of rock slices that are the counterparts of the thin sections studied. These analyses were performed by W. B. Stern using a non-destructive energy-dispersive X-ray fluorescence equipment (Tracor Spectrace-5000) at Basel University. The data were normalized to 100%. The purpose of these analyses was to assess wether only major elements played a role during metamorphism, or wether other elements were important too (see also later).

Geological framework

The Penninic nappes of the eastern part of the Lepontine area (Central Alps, Switzerland) were piled up during the Eocene and the Oligocene (SCHMID et al., 1990; for a detailed discussion, see
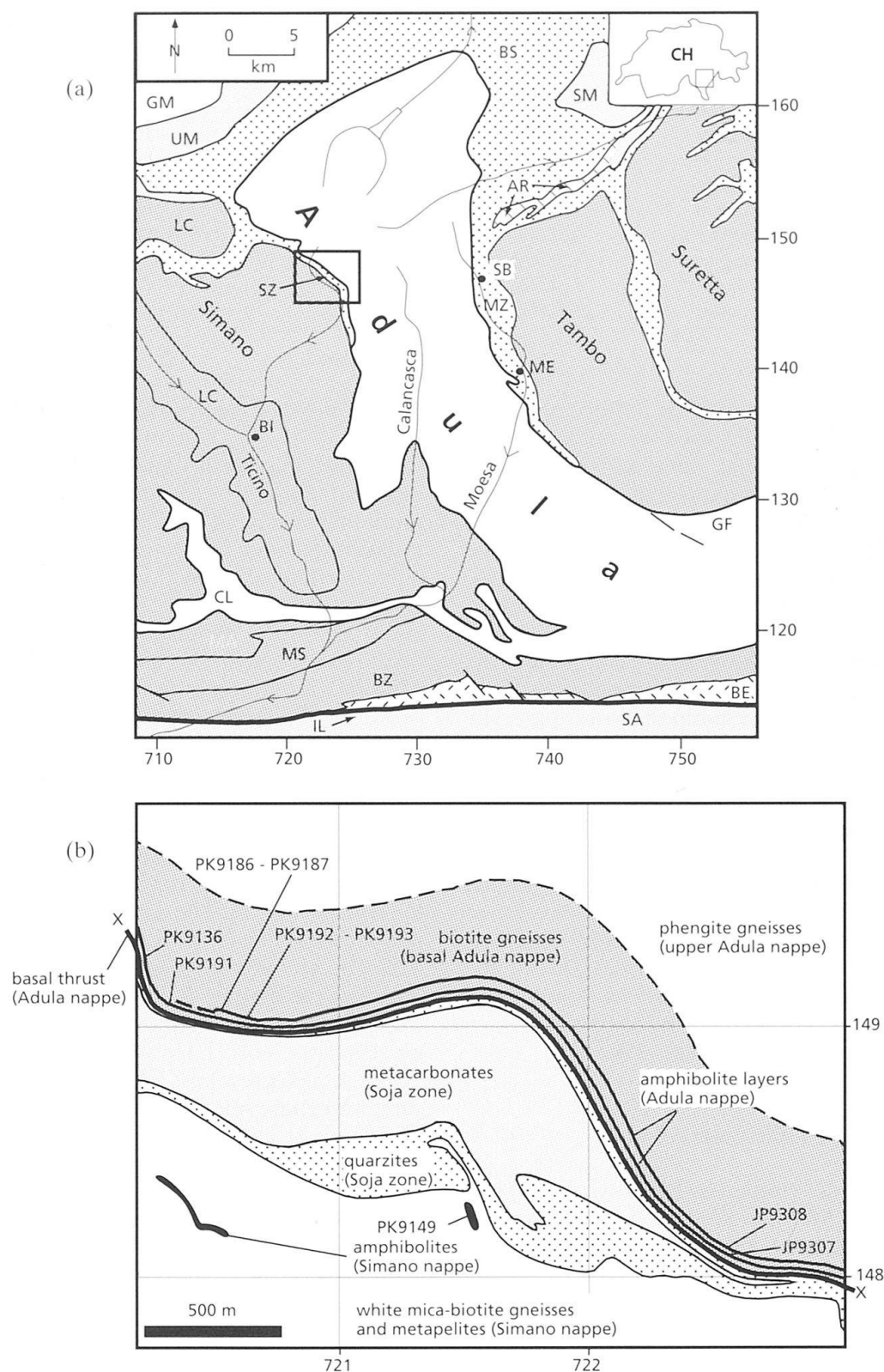
Fig. 1 (a) Simplified tectonic map of the Adula nappe and adjacent units. Inset map = Switzerland. Numbers on either side of map mark Swiss coordinate system. Square refers to figure 1b.
Abbreviations: AR: Areua slices, BE: trail of Bergell pluton, BS: Bündnerschiefer including Misox zone (MZ) and Soja zone (SZ), BZ: Bellinzona zone; CL: Cima Lunga unit, GF: Gruf massif, GM: Gotthard massif, IL: Insubric line, LC: Lucomagno, MA: Maggia zone, MS: Mergoscia zone, SA: Southern Alps, SM: Schams nappes, UM: Mesozoic cover (Gotthard massif), BI: Biasca, ME: Mesocco, SB: San Bernardino.
(b) Simplified geological map of the study area modified after KRUSPAN (1993). Sample locations are indicated. Numbers on either side of map mark Swiss coordinate system. Note, amphibolite layers (Adula nappe) not in scale.

Tab. 1   Mineral assemblage of amphibolites investigated in this study.

sample #	tectonic unit	Swiss coordinates	assemblage (+ qtz)
JP9307	Adula nappe	722.675/157.800	am + bt + plag + ilm + czo + cal+rt
JP9308	Adula nappe	722.675/157.800	am + bt + plag + ttn + czo + rt
PK9136	Adula nappe	721.230/149.080	am + grt + bt + plag + rt + ilm + czo + cal
PK9149	Simano nappe	721.520/148.410	am + bt + plag + ilm + czo + cal + rt
PK9186	Adula nappe	720.560/149.110	am + grt + bt + plag + ttn + ilm + czo
PK9187	Adula nappe	720.560/149.110	am + grt + bt + plag + ttn + ilm + czo
PK9191	Adula nappe	720.570/149.110	am + bt + plag + rt + ilm + czo + cal
PK9192	Adula nappe	720.600/149.130	am + bt + plag + ttn + ilm + czo
PK9193	Adula nappe	720.600/149.130	am + bt + plag + ttn + ilm + czo

SCHMID et al., 1996). During and after nappe formation and stacking, this area was affected by a Barrovian-type regional metamorphism. The Adula and the Simano nappes, separated by the Soja zone, belong to the structurally lower part of this pile (Fig. 1a). The Soja zone represents the former autochthonous cover of the Simano nappe. The base of the Adula nappe is dominated by biotite-bearing gneisses. Amphibolites occur as thin layers (Fig. 1b). Eclogites are common in the upper part of the Adula nappe (HEINRICH, 1986) but apparently do not occur in the lower part. The Soja zone consists of Mesozoic quartzites and metacarbonates (Fig. 1b). The upper part of the Simano nappe is characterized by mica gneisses and metapelites with a few intercalated amphibolite layers.

The rocks in the study area display a mylonitic foliation S4, which contains a well developed streching lineation L4. These structural elements were formed during the Leis phase (D4) of the Adula nappe contemporaneously with the thrusting of the Adula nappe onto the structurally lower units (PARTZSCH and MEYRE, 1995).

Sample description

Different samples studied by KRUSPAN (1993) and PARTZSCH and MEYRE (1994; 1995) were reinvestigated in this study. Sample numbers with the addition of PK are from KRUSPAN (1993); sample numbers beginning with JP are from PARTZSCH and MEYRE (1994; 1995) and PARTZSCH et al. (in prep.). Sample localities are shown in figure 1b. All samples were collected from amphibolite layers of about 1 m thickness that are coherently intercalated with gneisses. The gneiss assemblage includes plagioclase, white K-mica, biotite, quartz and opaques (± garnet). Table 1 lists the mineral assemblages of the amphibolite samples investigated in this study. In all samples, the relationship between mineral crystallization and rock deformation could be clearly established (Fig. 2, and below).

Optical microscopy and EMP showed that two different mineral reactions occurred in the amphibolites studied. (i) During development of the foliation S4 and in the presence of quartz and aqueous fluid, the reaction amphibole₁ + plagioclase₁ + biotite₁ + rutile → amphibole₂ + plagioclase₂ + biotite₂ + clinozoisite + titanite or ilmenite occurred in some of the samples. (ii) In other samples, the alteration must have occurred in the presence of quartz and a mixed H_2O-CO_2 fluid. In these samples, the reaction was amphibole₁ + plagioclase₁ + biotite₁ + rutile → amphibole₂ + calcite + plagioclase₂ + biotite₂ + clinozoisite + ilmenite. Amphibolites that indicate reaction (i) contain amphibole and minor amounts of biotite clasts (amphibole₁, biotite₁) that are wrapped by the foliation S4 (Fig. 3). The amphibole clasts contain plagioclase inclusions with an anorthite content of 0.28. The second type of amphibole (amphibole₂) occurs in the matrix. It defines the foliation fabric together with quartz, clinozoisite, biotite₂, and plagioclase₂ (an ~ 0.37). However, as shown in figure 2, biotite also grew post S4. In addition, in all rock samples rutile grains are armoured by aggregates of titanite or ilmenite. In amphibolites that show reaction (ii), amphibole₁ was mostly replaced by calcite. Amphibole₂ defines the foliation fabric together with quartz, clinozoisite, biotite₂, calcite, and plagioclase₂. In these rocks, biotite grew also during and after the development of the main foliation S4. Figure 4 shows the replacement texture of amphibole₁ by calcite. The image reveals that relics of amphibole₁ clasts were preserved during metamorphism. In one sample (JP9307), however, the replacement was found to be almost complete, and only trace amounts of amphibole clasts are present in this sample. All other samples contain larger amounts of relics of their protolith assemblages. Replacement of amphibole by calcite was observed in four different samples. Because these samples are located close to the adjacent metacar-

mineral	pre-Leis phase	Leis phase (D4)	post-Leis phase
biotite I			
biotite II			
biotite III			
calcite			
chlorite			
clinozoisite			
amphibole I			
amphibole II			
amphibole III			
ilmenite			
K-feldspar			
K-white mica			
plagioclase I			
plagioclase II			
plagioclase III			
quartz			
rutile			
titanite			

Fig. 2 Relation of mineral growth and deformation phase in samples JP9307 and JP9308. In this study only mineral generations I and II are discussed. The minerals of generation III will be treated in a subsequent paper (PARTZSCH et al., in prep.).

Fig. 3 Textural relationship between amphibole clasts and the phases in the matrix. The amphibole clasts are wrapped by the foliation, which is defined by matrix amphibole, biotite, clinozoisite, titanite (not shown), plagioclase, and quartz. Sample JP9308.
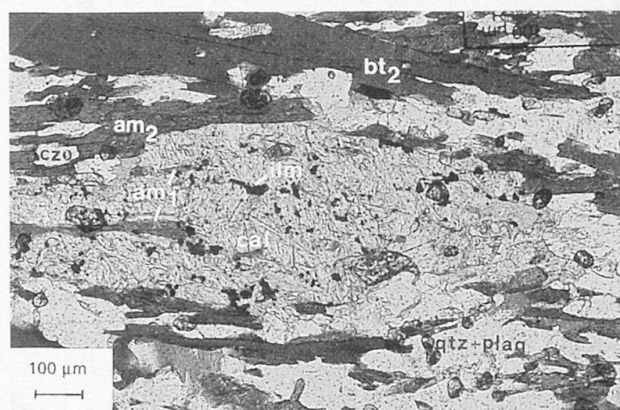
Fig. 4 Replacement textures of amphibole by calcite. Relics of amphibole clasts (amphibole$_1$) are indicated. Calcite grain is cigar-like shaped and smeared out into the foliation plane. Sample JP9307.

bonates of the Soja zone (see Fig. 1), we suggest that the Soja zone rocks released a mixed $H_2O–CO_2$ fluid. Observations of mineral textures (see above) reveal that the process of replacement occurred pre- to syn-kinematically with respect to the development of the foliation S4 (see Fig. 2). This is shown by the fact that calcite is smeared out parallel into the foliation plane, and that matrix amphiboles do not show any replacement features (Fig. 4). It has to be noted that in this paper the mineral generations I and II are discussed only. Mineral generation III will be treated in a later paper by PARTZSCH et al. (in prep.).

Mineral compositions and exchange vector analysis for amphibole

Compositions of minerals were obtained from samples JP9307 and JP9308 using EMP. Representative selected analyses for amphibole, biotite, clinozoisite, and plagioclase are listed in table 2.

Calcite was found to be pure $CaCO_3$, and therefore analyses are not presented. Small compositional variations were found in clinozoisite. Plagioclase displays a significant increase in X_{an} from grains of the first generation to those of the second generation (see Tab. 2). The most significant compositional variations were found between amphibole clasts and matrix amphiboles. Because these minerals are important for the interpretation of the metamorphic evolution of these rocks, they were investigated in more detail.

Substitutions in minerals can be detected from correlation matrices of cation proportions, or from exchange vector analysis. In this study the second procedure was used to monitor the compositional variations in amphibole of samples JP9308 and JP9307. In order to calculate the content of ferric iron in the amphibole structure, the method of STOUT (1972) was applied. As recom-

Tab. 2 Representative chemical analyses of important minerals from samples JP9307 and JP9308, respectively. $_1$ or $_2$ indicate generation of mineral (see text). Cl, F in amphibole is below detection limit as measured by energy dispersive spectrometry.
Abbreviations: d.l. = below detection limit.

Sample #	JP9307 biotite$_2$	JP9307 biotite$_2$	JP9307 czo	JP9307 plag$_2$	JP9307 plag$_2$	JP9307 plag$_1$	JP9307 plag$_1$	JP9307 am$_2$ (matrix)	JP9307 am$_2$ (matrix)	JP9308 biotite$_2$ (matrix)	JP9308 biotite$_3$ (post-matrix)	JP9308 czo	JP9308 plag$_2$	JP9308 plag$_2$	JP9308 plag$_1$	JP9308 plag$_1$	JP9308 am$_1$ (clast)	JP9308 am$_2$ (matrix)
SiO$_2$	35.70	35.70	38.10	62.89	61.97	63.42	63.78	44.23	44.23	38.11	37.28	39.79	58.94	58.70	61.86	60.84	47.61	47.38
TiO$_2$	1.89	1.44	0.20	d.l.	d.l.	d.l.	0.01	0.53	0.33	1.53	1.49	0.02	0.01	0.03	0.01	0.02	0.30	0.32
Al$_2$O$_3$	17.21	16.64	26.79	23.34	23.85	23.05	22.63	13.98	12.53	16.42	16.25	31.28	25.98	25.46	23.85	24.52	10.46	12.85
FeO	22.82	21.61	8.17	0.15	0.32	0.39	0.34	20.65	19.69	14.96	16.27	2.38	0.21	0.29	0.28	0.16	12.34	12.93
MnO	0.33	0.31	0.47	d.l.	d.l.	d.l.	d.l.	0.34	0.37	0.07	0.12	0.05	0.02	0.08	d.l.	0.01	0.27	0.21
MgO	9.09	10.11	0.04	d.l.	d.l.	0.01	d.l.	6.65	7.37	13.70	14.77	0.03	0.01	d.l.	d.l.	d.l.	12.78	11.91
Cr$_2$O$_3$	d.l.	d.l.	d.l.	0.06	d.l.	d.l.	d.l.	d.l.	0.00	d.l.	d.l.	0.01	0.01	d.l.	0.05	d.l.	0.08	0.22
CaO	0.05	0.04	23.23	4.55	5.69	3.69	3.51	11.05	10.89	0.07	0.08	24.70	7.63	7.70	5.79	6.83	12.20	10.97
K$_2$O	9.55	9.63	d.l.	0.17	0.01	0.08	0.07	0.61	0.52	0.09	0.08	0.02	0.12	0.07	0.10	0.12	0.25	0.23
Na$_2$O	0.15	0.12	d.l.	9.18	8.55	9.55	9.78	1.26	1.27	10.80	9.58	0.02	7.15	7.01	8.12	7.74	0.71	1.10
Sum	96.79	95.60	97.00	100.34	100.48	100.19	100.12	97.30	97.20	95.75	95.92	98.38	99.17	99.34	100.04	100.24	97.00	98.12
Si	5.46	5.50	3.00	2.78	2.74	2.80	2.82	6.34	6.61	5.68	5.56	3.02	2.65	2.64	2.74	2.70	6.89	6.72
Ti	0.22	0.17	0.01	d.l.	d.l.	d.l.	d.l.	0.06	0.04	0.17	0.17	d.l.	d.l.	d.l.	d.l.	d.l.	0.03	0.03
Al^{tot}	3.10	3.02	2.49	1.22	1.24	1.20	1.18	2.47	2.21	2.89	2.86	2.80	1.33	1.35	1.25	1.28	1.78	2.15
Fe^{2+}	2.92	2.79	0.48	0.01	0.01	0.01	0.01	1.98	2.01	1.86	2.03	0.14	0.01	0.01	0.01	0.01	1.15	1.20
Fe^{3+}								0.68	0.50								0.38	0.37
Mn	0.04	0.04	0.03	d.l.	d.l.	d.l.	d.l.	0.04	0.05	0.01	0.02	d.l.	d.l.	d.l.	d.l.	d.l.	0.03	0.03
Mg	2.07	2.32	0.01	d.l.	d.l.	d.l.	d.l.	1.49	1.64	3.04	3.28	d.l.	d.l.	d.l.	d.l.	d.l.	2.76	2.52
Cr	d.l.	d.l.	d.l.	d.l.	d.l.	0	d.l.	d.l.	0.00	d.l.	d.l.	0.01	d.l.	d.l.	d.l.	d.l.	0.01	0.02
Ca	0.01	0.01	1.96	0.22	0.27	0.18	0.17	1.78	1.75	0.01	0.01	2.01	0.37	0.37	0.28	0.33	1.89	1.67
Na	0.04	0.04	d.l.	0.79	0.73	0.82	0.84	0.37	0.37	0.03	0.02	d.l.	0.62	d.l.	0.01	0.01	0.20	0.30
K	1.86	1.89	d.l.	0.01	0.01	0.01	d.l.	0.12	0.10	2.05	1.82	d.l.	0.01	0.61	0.70	0.67	0.05	0.04
Σ Cations	15.73	15.78	7.97	5.01	5.01	5.01	5.02	15.33	15.26	15.75	15.77	7.98	5.00	4.99	4.98	4.99	15.18	15.05

Tab. 3 Exchange vectors used in this study. The concentration of each vector per 23 oxygens was calculated for each amphibole EMP analysis obtained during the course of this study.
Note: Abbreviations correspond to exchange vectors.

Name	concentration $X_{(ex)}$	
FM	$X_{(Fe^{2+}Mg_{-1})}$	$= Fe^{2+}$
ferri	$X_{(Fe^{3+}Al_{-1})}$	$= Fe^{3+}$
–	$X_{(MnMg_{-1})}$	$= Mn$
–	$X_{(MgCa_{-1})}$	$= -\dfrac{13}{46}(Na + K) - \dfrac{13}{23}Ca - \dfrac{3}{23}(Si + Ti) + \dfrac{7}{46}Al + \dfrac{10}{23}(Mg + Mn + Fe^{2+}) + \dfrac{7}{23}Fe^{3+}$
pa	$X_{(NaK_{-1})}$	$= -K$
ed	$X_{(ed)}$	$= \dfrac{31}{46}(Na + K) - \dfrac{7}{23}(Si + Ti) + \dfrac{1}{46}Al + \dfrac{8}{23}(Mg + Ca + Mn + Fe^{2+}) + \dfrac{1}{46}Fe^{3+}$
pl	$X_{(pl)}$	$= \dfrac{15}{46}(Na + K) + \dfrac{7}{23}(Si + Ti) - \dfrac{1}{46}Al - \dfrac{8}{23}(Mg + Ca + Mn + Fe^{2+}) - \dfrac{1}{46}Fe^{3+}$
ts	$X_{(ts)}$	$= -\dfrac{4}{23}(Na + K) + \dfrac{8}{23}Si + \dfrac{30}{23}Ti + \dfrac{20}{46}Al - \dfrac{8}{23}(Mg + Ca + Mn + Fe^{2+}) + \dfrac{11}{23}Fe^{3+}$
exti	$X_{(exti)}$	$= Ti$
additive	$X_{(Ca_2Mg_5Si_8O_{23}(OH)_2)}$	$= \dfrac{1}{46}(Na + K) + \dfrac{2}{23}(Si + Ti) + \dfrac{3}{46}(Al + Fe^{3+}) + \dfrac{1}{23}(Mg + Ca + Mn + Fe^{2+})$

mended by ROBINSON et al. (1982) for calcic amphiboles, the cations $Si + Ti + Al + Fe + Mg$ per formula unit (p.f.u.) were summed to 13 omitting Ca and Na. Iron then was redistributed between ferric and ferrous iron to bring the sum of oxygens p.f.u. to 23. In order to investigate the substitutions operating in amphibole, the cation proportions calculated from EMP data were transformed into one additive component and nine exchange vectors. The procedure presented here was outlined by FERRY (1984) and THOMPSON (1982a), and is described in some detail below. The exchange vector concept is a useful way to describe the chemical substitutions that occur in minerals. In composition space, an exchange vector possesses a direction and a magnitude or concentration. The choice of exchange vectors is arbitrary (THOMPSON, 1982a), and there are numerous ways in which they may be defined. However, in rock-forming minerals there are only a few common exchange vectors that describe the compositional relations between the endmembers of a specific mineral group. In general, it is not important which set of exchange vectors is used as long as the set i) completely describes the composition space, and ii) the vectors are linearly independent (THOMPSON, 1982a). For example, in order to describe a specific point within the composition space spanned by the endmembers tremolite $[Ca_2Mg_5Si_8O_{22}(OH)_2]$, edenite $[NaCa_2Mg_5AlSi_7O_{22}(OH)_2]$, pargasite $[NaCa_2Mg_4Al_2Si_6O_{22}(OH)_2]$,

tschermakite $[Ca_2Mg_3Al_4Si_6O_{22}(OH)_2]$, and their Fe counterparts, only three exchange vectors are needed. Although these endmembers are related to each other by numerous exchange vectors that can be found by subtracting the chemical formula of one endmember from another, most of the resulting vectors are not linearly independent. For example, $Ca_2Mg_5Si_8O_{22}(OH)_2 - Ca_2Mg_3Al_4Si_6O_{22}(OH)_2 = Mg_{-2}Si_{-2}Al_4$ or $Mg_{-1}Si_{-1}Al_2$, and for the Fe counterparts, $Ca_2Fe_5Si_8O_{22}(OH)_2 - Ca_2Fe_3Al_4Si_6O_{22}(OH)_2 = Fe_{-2}Si_{-2}Al_4$ or $Fe_{-1}Si_{-1}Al_2$. The $FeMg_{-1}$ exchange vector relates each Mg endmember to its Fe counterpart. The $Mg_{-1}Si_{-1}Al_2$ and $Fe_{-1}Si_{-1}Al_2$ exchange vectors are not linearly independent from each other, because $Mg_{-1}Si_{-1}Al_2 = Fe_{-1}Si_{-1}Al_2 + FeMg_{-1}$. In our example, the $Si_{-1}NaAl$, the $Mg_{-1}Si_{-1}Al_2$, and the $FeMg_{-1}$ vectors plus one additive component, say tremolite, sufficiently describe the compositions of the seven remaining endmembers as well as each point that lies within this composition space. A set of exchange vectors similar to that used by FERRY (1984) for biotite with the addition of the $Fe^{3+}Al_{-1}$ (ferri) exchange component was applied to amphibole investigated in this study. The additive component in this exchange vector set is, as in the example above, tremolite. The concentrations of the various exchange vectors in one mole of additive component are found by using the inverse of the composition matrix that consists of the additive component and the exchange vectors shown in table 3.
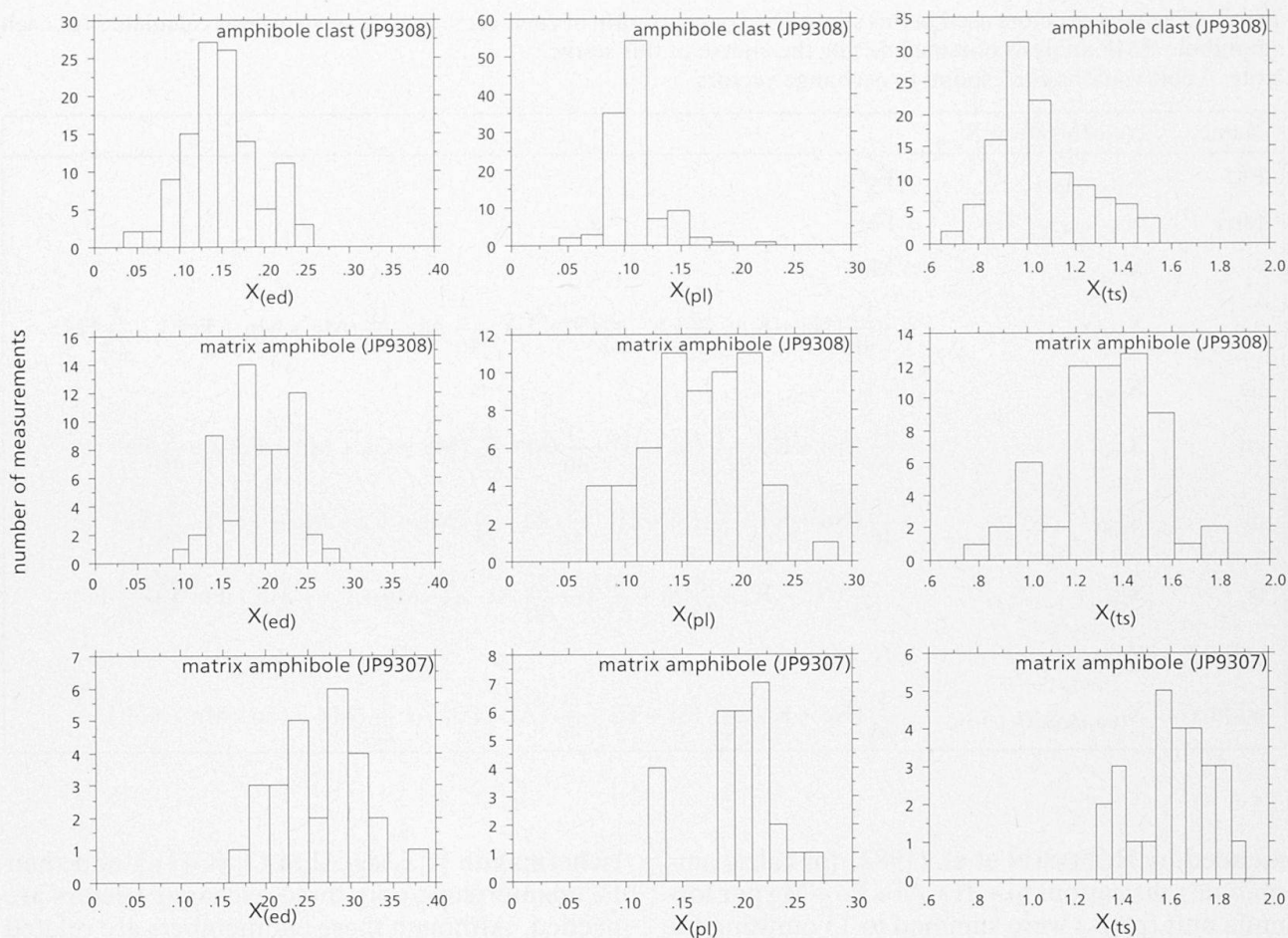
Fig. 5   Histograms for various exchange vectors applied to amphibole clasts and matrix amphiboles from samples JP9307 and JP9308, respectively. For discussion see text.

There are nine equations that relate the different exchange vectors and the additive component to the different system components, e.g., $Mg_{-1}Si_{-1}Al_2$ = 2Al – Si – Mg. By transforming these equations into matrix notation and inverting the matrix leads to the equations shown in table 3 (for details of the procedure, the reader is referred to Thompson, 1982a). The concentrations of the different exchange vectors X_{ex} per 23 oxygens may then be calculated from the equations in table 3.

The procedure outlined above generally reveals the following order of significance of the different exchange vectors in amphibole from both samples JP9307 and JP9308: ts, FM, ferri, ed, pl, $MgCa_{-1}$, pa. Other exchange vectors, such as for example, the exti vector or the $MnMg_{-1}$ substitution, are not significant. A comparison between the compositional variations in amphibole of the clast with those of the matrix (JP9308) showed that the FM exchange vector has approximately equal significance in both matrix amphiboles and clasts. The same is true for the $MgCa_{-1}$ component. The concentrations of the exchange components

ts, pl, and ed are presented in histograms (Fig. 5). The concentrations of these components are larger in the matrix amphiboles than in the cores of the amphibole clasts (Fig. 5). A profile through an amphibole clast reveals that the rims show compositions similar to those of the matrix amphiboles. The increase in the ts, pl, and ed exchange components from the core to the rim of the amphibole grain is shown in figure 6. A slight increase in the concentration of the ferri and a decrease in the pa exchange vectors is also observed along this direction. As mentioned above trace amounts of amphibole clasts occur also in sample JP9307. However, no differences in composition between the matrix amphibole and relics of amphibole clasts from this sample were observed. A comparison between the data of the matrix amphiboles from sample JP9308 with those from sample JP9307 shows that the concentrations of all exchange components are larger in the latter (see also Fig. 5). Summarizing these results, in terms of endmembers of the tremolite-tschermakite join, the matrix amphiboles from both samples are rich
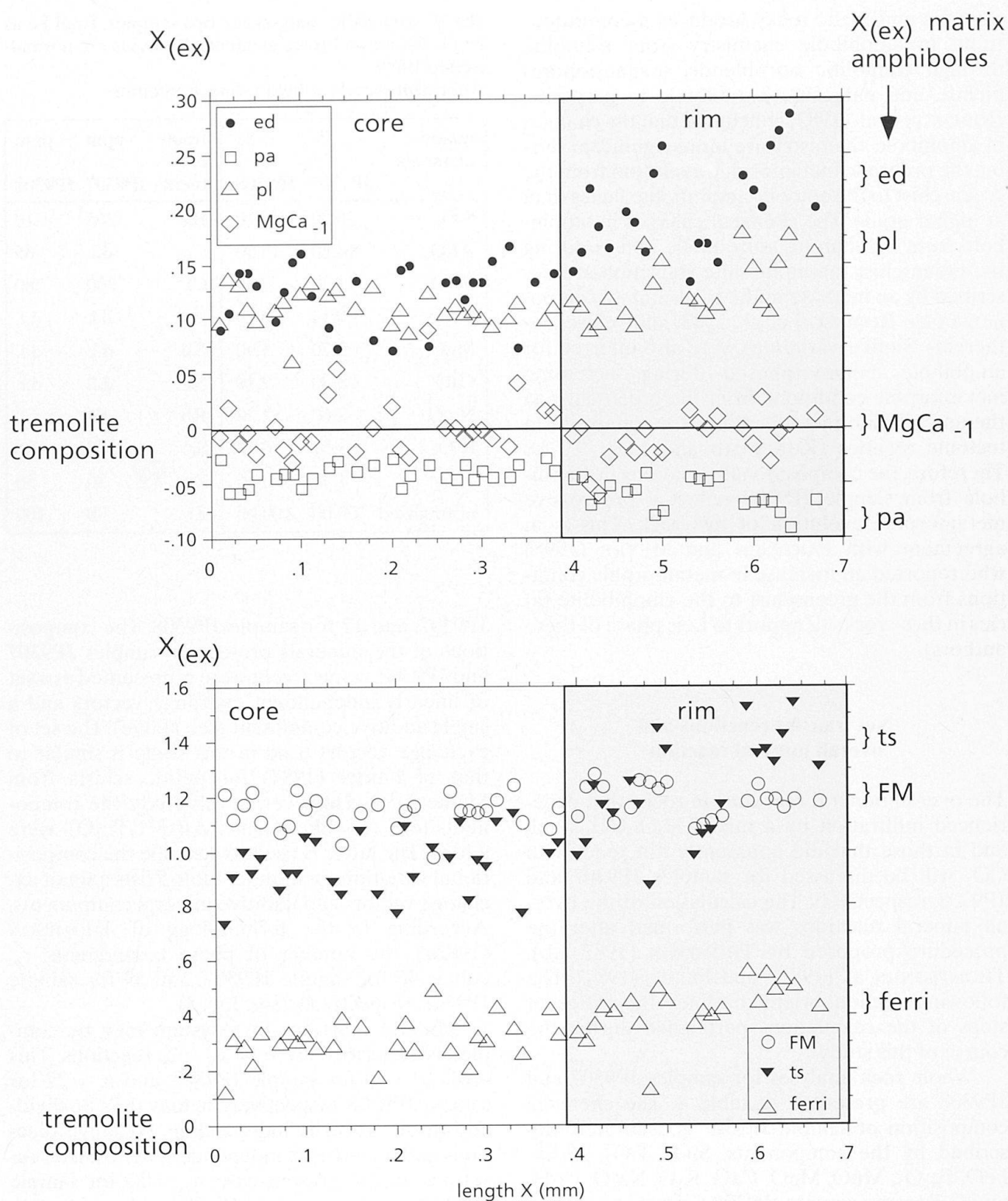
Fig. 6 Profile through core and rim region of amphibole clast from sample JP9308. Note the increase in ed, pl, ts, and the decrease in ferri and pa exchange vectors from core to rim. The x-axis of the plot represents distance, the y-axis the concentration of each exchange vector per 23 oxygens.

in tschermakite component. Clasts in sample JP9308 are rich in tremolite component.

The compositional variations in amphibole during prograde metamorphic evolution from the

greenschist to the epidote-amphibolite facies, and from the latter to the amphibolite facies were summarized by ROBINSON et al. (1982). According to these authors, progressive metamorphism of ul-

tramafic and mafic rocks produces a continuous trend in amphibole chemistry from tremolite through tremolitic hornblende, magnesiohornblende, and pargasitic hornblende to pargasite. ROBINSON et al. (1982) concluded that the changes in amphibole chemistry are more significant during the prograde metamorphic evolution from the greenschist to the epidote-amphibolite facies than at higher grade. The chemical changes in amphibole from medium pressure mafic schists during the greenschist to amphibolite transition are described by an increase in the ts, pl, and ed components (see ROBINSON et al., 1982, and references therein). Similar variations were also inferred for amphibole metamorphosed during increasing metamorphic conditions from the greenschist to the amphibolite facies in contact metamorphism tectonic regimes (KUNIYOSHI and LIOU, 1976). Therefore, the compositional variations in amphibole from sample JP9308 reflect a progressive metamorphic evolution of this rock. This is in agreement with PARTZSCH and MEYRE (1995) who reported an increase in metamorphic conditions from the greenschist to the amphibolite facies in these rocks (Zapport to Leis phase of these authors).

Net transfer reactions and overall mineral reaction

The overall mineral reactions in rocks that experienced infiltration by a mixed H_2O–CO_2 fluid, and in those that did apparently not react with CO_2 will be discussed for samples JP9307 and JP9308, respectively. The calculation of the overall mineral reactions was performed after the procedure proposed by THOMPSON (1982 a,b), THOMPSON et al. (1982), and FERRY (1984). The following section briefly outlines the different steps of the calculations performed during the course of this study.

Whole rock analyses for samples JP9307 and JP9308 are presented in table 4. The chemical composition of sample JP9307 is accurately described by the components: SiO_2, TiO_2, Al_2O_3, FeO, Fe_2O_3, MnO, MgO, CaO, K_2O, Na_2O, O, H, and C. Because sample JP9308 did not experience CO_2 metasomatism, its chemical composition may be described by the same components without C. Only major oxides were considered. Trace elements as those listed in table 4 are thought to play a minor role during metamorphism of the rocks, and therefore, were neglected for simplicity. According to THOMPSON (1982a), the above components may be called system components c_s. In the present case, they are 13 in number for sample

Tab. 4 ED-XFR analyses for two samples. Total Fe as Fe_2O_3. Minor and trace elements. Analyses are normalized to 100%.
Abbreviations: d.l. = below detection limit.

major elements	% JP9307	% JP9308	trace elements	ppm JP9307	ppm JP9308
SiO_2	56.30	58.10	Ba	265	210
Al_2O_3	14.20	15.50	Ce	d.l.	65
Fe_2O_3	11.28	7.39	Cr	290	280
MnO	0.14	0.13	As	d.l.	d.l.
MgO	3.70	5.90	Nb	d.l.	d.l.
CaO	8.80	9.40	Ni	d.l.	d.l.
Na_2O	2.60	2.10	Rb	66	d.l.
K_2O	1.51	0.78	Sr	77	186
TiO_2	1.37	0.66	Zn	80	50
normalized	100.00	100.00	Zr	70	100

JP9307, and 12 for sample JP9308. The compositions of the minerals present in samples JP9307 and JP9308, respectively, were represented as a set of linearly independent exchange vectors and a single additive component (see above). The set of exchange vectors used in this study is similar to that of FERRY (1984) for pelitic schists from Maine, USA. However, in this study, the components ferri (see above), and $Al(OH)Ti_{-1}O_{-1}$ were added. The latter is used to describe the compositional variations in titanite. Table 5 lists a set of exchange vectors and additive mineral components. According to the terminology of THOMPSON (1982a), the number of phase components, c_p, equals 46 for sample JP9307, and 39 for sample JP9308, respectively (see Tab. 5).

Mineral reactions in a system may be completely described by $n_r = c_p - c_s$ reactions. This gives $n_r = 33$ for sample JP9307, and $n_r = 27$ for sample JP9308, respectively. n_r may then be divided into n_{ex} linearly independant exchange reactions and n_{nt} linearly independent net transfer reactions. In the present case, $n_{ex} = 25$ for sample JP9307 and 20 for sample JP9308 and $n_{nt} = n_r - n_{ex}$, which results in 8 and 7 linearly independent net transfer reactions for samples JP9307 and JP9308, respectively. Table 6 lists a set of net transfer reactions for both samples. With the exception of SiO_2, CO_2, and H_2O, each net transfer reaction involves the additive component of a different phase. Net transfer reactions completely describe the growth and consumption of a mineral or fluid phase. Exchange reactions change the compositions of min-

Tab. 5 Exchange vectors and additive components used in this study.

additive component	exchange vectors
calcite	$MgCa_{-1}$, $MnMg_{-1}$, FM
clinozoisite	ferri
ilmenite	FM, $MnMg_{-1}$
phlogopite	FM, ed, pa, pl, $MnMg_{-1}$, ts, exti, $MgCa_{-1}$
plagioclase	pl
titanite	ferri, $Al(OH)Ti_{-1}O_{-1}$
tremolite (= am_1)	FM, ferri, ed, pa, pl, $MnMg_{-1}$, ts, exti, $MgCa_{-1}$
tschermakite (= am_2)	FM, ferri, ed, pa, pl, $MnMg_{-1}$, ts, exti, $MgCa_{-1}$
rutile	
quartz	
CO_2	
H_2O	

Tab. 6 Net transfer reactions used to describe the overall mineral reaction: Net transfer reactions with * were used for sample JP9307. Net transfer reactions with ** were applied to sample JP9308.

k	net transfer reactions
1*,**	plag = 4 qtz + ed + pl
2*	cal + ½ pl + ½ $MgCa_{-1}$ + ½ ts = ½ qtz + ½ ed + CO_2
3*	ilm + H_2O = 2 qtz + FM + 2 ts + 3 exti + 2 $Al(OH)Ti_{-1}O_{-1}$
4**	ttn + ½ $MgCa_{-1}$ + ½ pl = ½ qtz + ½ ed + ½ ts + exti
5*,**	phl + pa + ¾ pl + ¾ ts = ¹¹⁄₄ qtz + H_2O + ¾ ed + ¾ $MgCa_{-1}$
6*,**	zo + ¼ pl + ¼ $MgCa_{-1}$ + ¼ ts = ²⁵⁄₄ qtz + ½ H_2O + ¼ ed
7*,**	tr + ½ pl + ½ ts = ²³⁄₂ qtz + H_2O + ½ ed + ½ $MgCa_{-1}$
8*,**	tsch + ½ pl + ½ ts = ²³⁄₂ qtz + H_2O + ½ ed + ½ $MgCa_{-1}$
9*,**	rt = qtz + exti + ts

erals, as shown for example for amphibole, but do not alter their modal abundances. Thus, the progress of the net transfer reactions may be used to determine the complete mineral reaction that occurred in a rock (FERRY, 1984). In this study, the progress of the net transfer reactions shown in table 6 was measured for samples JP9307 and JP9308, respectively.

The reaction progress of each net transfer reaction was determined as follows. Volume amounts of minerals were measured as described in a previous section. Volume amounts were converted to molar amounts using the volume data by HOLLAND and POWELL (1990). The mineralogical composition of the protolith was reconstructed by assuming an isochemical alteration with the exception of a CO_2–H_2O fluid that was added to the rock. Modal abundances of the minerals of the protolith may be calculated using equation 1 (see also FERRY, 1984).

$$\sum(\alpha_{i,j}n_j)_{product} = \sum(\alpha_{i,j}n_j)_{educt} \quad (1),$$

where $a_{i,j}$ is the number of atoms p.f.u. of element i in mineral j, and n_j is the number of moles of mineral j. In samples JP9307 and JP9308, i = (Si + Al), Ti, (Na + Ca), K, and (Fe^{2+} + Fe^{3+} + Mg + Mn). As determined by optical microscopy and EMP (see previous section), j of the protolith (educt) is biotite$_1$, amphibole$_1$, plagioclase$_1$, rutile, and quartz. Minerals j on the left hand side of the expression

were biotite$_2$, amphibole$_2$, plagioclase$_2$, clinozoisite, calcite, ilmenite, and quartz for sample JP9307. For sample JP9308, calcite was omitted and ilmenite was replaced by titanite.

In order to solve equation (1) for n_{jeduct}, the compositions of the protolith minerals have to be known. Because the alteration in sample JP9307 was complete, the mineral compositions of the protolith had to be estimated. As a first approach, we assumed that the differences in composition between plagioclase 1 and 2, and amphibole 1 and 2 (see before) from sample JP9308 are similar to those that existed between each different mineral generations from sample JP9307. Thus, the compositions were calculated from:

$$\Delta\alpha_{i,j\,(product-educt)}\,JP9308 = \\ = \Delta\alpha_{i,j\,(product-educt)}\,JP9307 \quad (2),$$

with i = Si, Al, Ti, Fe^{2+}, Fe^{3+}, Mg, Mn, Na, Ca, K, and j = amphibole, and plagioclase. The procedure presented above was not applied to biotite, because trace amounts of relics of the first biotite generation were found in thin sections prepared for optical microscopy only. For simplicity we assumed that the compositional differences between the different biotite generations were small. Modal amounts of minerals of the different samples under investigation and of the reconstructed protoliths of samples JP9307 and JP9308 are listed in table 7. The different amphibole generations (amphibole$_1$ and amphibole$_2$) were

Tab. 7 Volume amounts and number of moles for minerals of different samples per 1000 cm³ and protoliths of samples JP9307, and JP9308. * denotes the protolith compositions. Volume data for minerals are from HOLLAND and POWELL (1990). Volume data used for minerals that show solid solutions such as garnets are given in brackets.

	calcite	clinozoisite	ilmenite	phlogopite	plagioclase	titanite	am clast	matrix am	quartz	garnet	white K-mica	rutile
Volume data	36.89	135.80	31.69	149.64	100.79 (an)	55.65	272.70 (tr)	268.80 (tsch)	22.69	115.51 (grs)	140.83 (ms)	18.82
JP9307 cm³	48.22	12.89	2.01	97.67	130.02			517.70	170.40			
n(moles)	1.307	0.102	0.063	0.652	1.280			1.925	7.510			
JP9307p* cm³												
n(moles)				0.676	2.809		1.899		2.914			0.064
PK9136 cm³	41.10	35.00	2.00	325.50	121.60	2.53	255.44		216.83			
n(moles)	1.114	0.258	0.063	2.175	1.206	0.045	0.937		9.556			
JP9308 cm³		54		61.5	51.5	7	227.5	390	205			3.5
n(moles)		0.398		0.411	0.511	0.126	0.834	1.451	9.035			0.180
JP9308* cm³												
n(moles)				0.359	0.950		2.339		8.458			0.315
PK9191 cm³	138	102.5	9.5	194.5	96		41		233	24.5	162	
n(moles)	3.741	0.755	0.300	1.300	0.953		0.151		10.269	0.213	1.150	
PK9149 cm³	88.5	76.5	2.5	252	198.5		42	160.5	175.5			4
n(moles)	2.399	0.563	0.079	1.684	1.969		0.154	0.597	7.735			0.213

counted separately because they could be readily distinguished in thin section. The different plagioclase generations, however, were impossible to differentiate. Biotite$_1$ and biotite$_2$ could also be distinguished in these samples. However, the number of biotite$_1$ grains is so small (~ three per thin section) that they did not enter the point counting statistics. Therefore, there is no number for volume amounts of biotite$_1$ in table 7.

The progress x of the different net transfer reactions listed in table 6 may be determined by
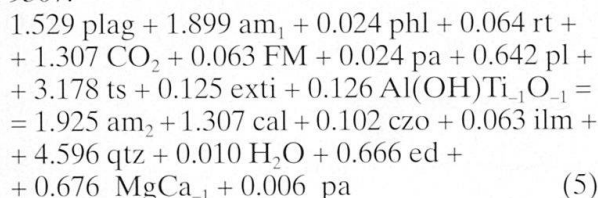
$$\xi = n_{j,k(product)} - n_{j,k(educt)} \tag{3},$$

where $n_{j,k}$ is the number of additive mineral component j of the net transfer reaction k. The overall mineral reaction for a rock may then be calculated from expression (4) (see FERRY, 1984).
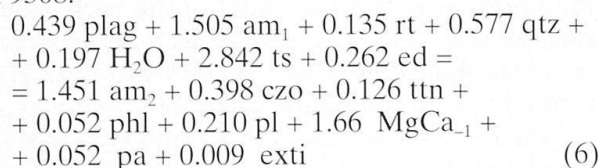
$$\sum_k \{\sum_j v_j(j)\xi_k\} = 0 \tag{4},$$

where v_j is the stoichiometric coefficient of the species j in the k th net transfer reaction. ξ values for the different net transfer reactions for specimens JP9307 and JP9308 are presented in table 8. The overall mineral reactions for the two specimens are:

JP9307:
  1.529 plag + 1.899 am$_1$ + 0.024 phl + 0.064 rt + + 1.307 CO$_2$ + 0.063 FM + 0.024 pa + 0.642 pl + + 3.178 ts + 0.125 exti + 0.126 Al(OH)Ti$_{-1}$O$_{-1}$ = = 1.925 am$_2$ + 1.307 cal + 0.102 czo + 0.063 ilm + + 4.596 qtz + 0.010 H$_2$O + 0.666 ed + + 0.676 MgCa$_{-1}$ + 0.006 pa (5)

JP9308:
  0.439 plag + 1.505 am$_1$ + 0.135 rt + 0.577 qtz + + 0.197 H$_2$O + 2.842 ts + 0.262 ed = = 1.451 am$_2$ + 0.398 czo + 0.126 ttn + + 0.052 phl + 0.210 pl + 1.66 MgCa$_{-1}$ + + 0.052 pa + 0.009 exti (6)
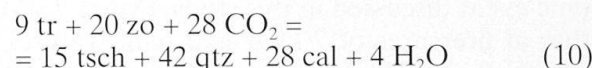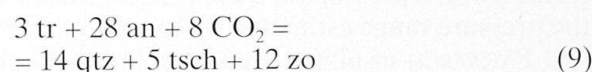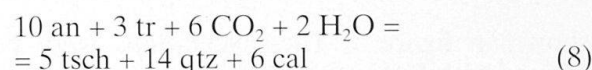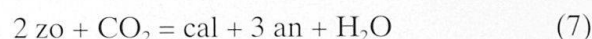
The reaction that occurred in sample JP9307 is a carbonation-dehydration reaction caused by the infiltration of a mixed H$_2$O–CO$_2$ fluid. Reaction (5) suggests that large amounts of CO$_2$ reacted with the sample, whereas H$_2$O from the infiltrating fluid did not react. Moreover, reaction (5) resulted in the production of small amounts of H$_2$O. Reaction (6) is a hydration reaction with only small amounts of H$_2$O that were consumed by the rock. Carbonation and/or hydration reactions always result in positive volume changes of the reaction products. Because higher amounts of CO$_2$ were consumed than amounts of H$_2$O were produced, sample JP9307 experienced an increase in the volume of the solids. An increase in volume of sample JP9308 is also indicated by reaction (6).

Tab. 8 Reaction progress ξ of the k = 1 through 9 net transfer reactions.

k	ξ JP9307	ξ JP9308
1	–1.529	–0.439
2	1.307	–
3	0.063	–
4	–	0.126
5	–0.024	0.052
6	0.102	0.398
7	–1.899	–1.505
8	1.925	1.451
9	–0.064	–0.135

Fluid rock interaction and fluid flux calculations

In order to determine the composition of the fluid in equilibrium with sample JP9307, isobaric temperature – $X_{CO_2}^{eq}$ phase diagrams were calculated. Calculations were performed using GEOCALC (BROWN et al., 1988) and the database of BERMAN (1988). This thermodynamic database was extended with data for tschermakite (MÄDER and BERMAN, 1992). Calculations were performed in the CMASH-CO$_2$ system. Four reactions were used to calculate the stability field of the assemblage calcite + matrix amphibole + biotite + plagioclase + ilmenite + quartz + clinozoisite. A subgroup of this assemblage may be represented by the phases listed in reactions (7) through (10), where the endmembers tsch and tr were used to model matrix amphibole. For the CO$_2$–H$_2$O fluid mixture, the equation of state by KERRICK and JACOBS (1981) was applied.

$$2 \text{ zo} + CO_2 = \text{cal} + 3 \text{ an} + H_2O \tag{7}$$

$$10 \text{ an} + 3 \text{ tr} + 6 \text{ CO}_2 + 2 \text{ H}_2O = = 5 \text{ tsch} + 14 \text{ qtz} + 6 \text{ cal} \tag{8}$$

$$3 \text{ tr} + 28 \text{ an} + 8 \text{ CO}_2 = = 14 \text{ qtz} + 5 \text{ tsch} + 12 \text{ zo} \tag{9}$$

$$9 \text{ tr} + 20 \text{ zo} + 28 \text{ CO}_2 = = 15 \text{ tsch} + 42 \text{ qtz} + 28 \text{ cal} + 4 \text{ H}_2O \tag{10}$$

Phases on the left hand side of the reactions are stable on the low X_{CO_2} side or on the high-temperature side. Activity-composition relationships for tr were taken from HOLLAND and POWELL (1990). For tschermakite a mixing model similar to that for tr by HOLLAND and POWELL (1990) was applied (see DALLA TORRE et al., 1996). Activity values for zoisite were computed using the mixing model by DROOP (1985). As mentioned above, calcite in sample JP9307 is pure CaCO$_3$, and therefore a$_{CaCO_3}$ = 1. Activity-composition relationships for anorthite were modeled assuming random mixing of Na and Ca, as well as of Al and Si (e.g., SPEAR, 1993). The results of the calculations are
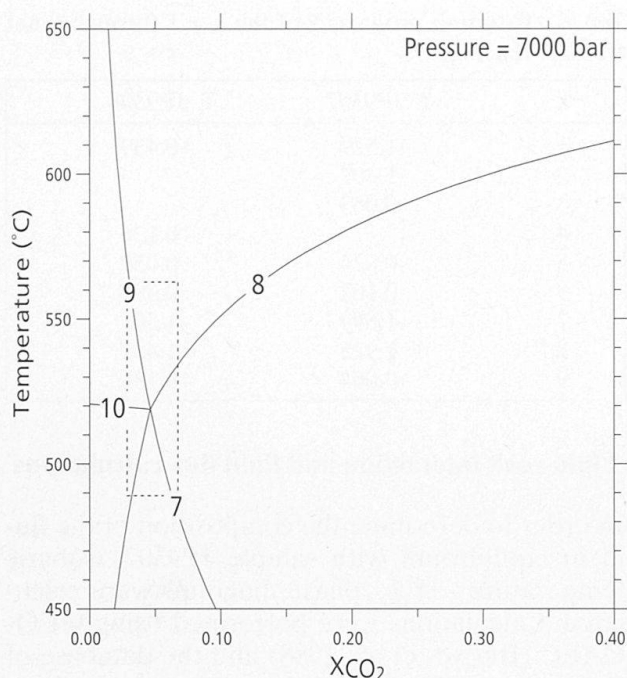
Fig. 7 Calculations in the CMASH-CO$_2$ system. At pressures of 7 kbar and temperatures of 520 °C, the equilibrium assemblage consists of cal + am + zo + plag + fluid. The mole fraction of CO$_2$ ($X^{eq}_{CO_2}$) in equilibrium with this assemblage is 0.05. Reactions used: (7) cal + 3 an + + H$_2$O = 2 zo + CO$_2$, (8) 10 an + 3 tr + 6 CO$_2$ + 2 H$_2$O = = 5 tsch + 14 qtz + 6 cal, (9) 3 tr + 28 an + 8 CO$_2$ = = 14 qtz + 5 tsch + 12 zo, (10) 9 tr + 20 zo + 28 CO$_2$ = = 15 tsch + 42 qtz + 28 cal + 4 H$_2$O. The error field was calculated by using the standard deviation of activity values of the different phases. The pressure and temperature range is consistant with that derived by PARTZSCH and MEYRE (1994) for the metamorphic event discussed in this study.

shown in figure 7. The calculations were performed with a pressure of 7 kbar. This value lies in the pressure range estimated by ENGI et al. (1995) and PARTZSCH et al. (in prep.) for the metamorphic event discussed in this study. Figure 7 shows that at pressures of 7 kbar and temperatures of 520 °C, the equilibrium assemblage consists of cal + am + zo + plag + fluid. The mole fraction of CO$_2$ ($X^{eq}_{CO_2}$) in equilibrium with this assemblage is 0.05. As shown in figure 7, because of variable activity values for the different phases, the standard deviation in temperature is relatively large (see Fig. 7). In contrast, the standard deviation in $X^{eq}_{CO_2}$ was found to be relatively small (see Fig. 7).

The calculations of the amount of fluid that infiltrated sample JP9307 is similar to that presented by RICE and FERRY (1982). If devolatilization reactions occur in a rock isolated from an external fluid source, the mineral assemblage in the rock has a large capacity to buffer the composition of the fluid (see also GREENWOOD, 1975). In this case,

rocks communicate only with small amounts of pore fluid that will be modified as the devolatilization reactions progress. According to the terminology of RICE and FERRY (1982), this mechanism is called "internal buffering". However, sample JP9307 experienced a carbonation reaction, and the fluid infiltrated from an external source. In this case, the fluid composition is controlled by the external reservoir and the local mineral reactions have little ability to control the fluid composition. Such situations are given when the external fluid reservoir is large relative to the buffering capacity of the local mineral assemblages. Under these conditions, the mineral reactions proceed by ajusting the mineralogy of the rock as well as the mineral composition toward an equilibrium with the rock (RICE and FERRY, 1982). Because $X^{eq}_{CO_2}$ is believed to be controlled by the composition of the fluid ($X^{ext}_{CO_2}$) from the external reservoir, $X^{eq}_{CO_2} = X^{ext}_{CO_2}$. The relations between the number of moles of CO$_2$ ($n^{ext}_{CO_2}$) and H$_2$O ($n^{ext}_{H_2O}$) that infiltrated the rock, and $X^{eq}_{CO_2}$ or $X^{ext}_{CO_2}$ during the progress of the overall mineral-fluid reaction are given in equations 11 through 13.

$$X^{eq}_{CO_2} = \frac{\Delta n_{CO_2}}{n^{ext}_{CO_2} + n^{ext}_{H_2O} + n^{flpore}_{CO_2} + n^{flpore}_{H_2O}} = X^{ext}_{CO_2} =$$

$$= \frac{n^{ext}_{CO_2}}{n^{ext}_{CO_2} + n^{ext}_{H_2O}} \qquad (11)$$

$$n^{ext}_{CO_2} = \Delta n_{CO_2} + n^{flout}_{CO_2} \qquad (12)$$

$$n^{ext}_{H_2O} = \Delta n_{H_2O} + n^{flout}_{H_2O} \qquad (13)$$

$n^{flpore}_{CO_2}$ and $n^{flpore}_{H_2O}$ are the number of moles of CO$_2$ and H$_2$O present in the pore fluid of the rock. Equations 12 and 13 are the mass conservation expressions for fluid flow of the species CO$_2$ and H$_2$O through the amphibolite layer. Δn_{CO_2} and Δn_{H_2O} are the number of moles of CO$_2$ and H$_2$O that reacted with the rock, $n^{flout}_{CO_2}$ and $n^{flout}_{H_2O}$ are the moles of CO$_2$ and H$_2$O that flowed through the rock without reacting with it. In the present case, it is assumed that rock porosity was very small, probably less than 0.1% (RICE and FERRY, 1982). Thus, the terms $n^{flpore}_{CO_2}$ and $n^{flpore}_{H_2O}$ are vanishingly small and can be neglected in the calculation. Very small values may also be assumed for $n^{flout}_{CO_2}$. This assumption is supported by the fact that the surrounding gneisses as well as all subsequent amphibolite layers record no reaction with CO$_2$. For simplification, we suggest that $n^{flout}_{CO_2} = 0$. With these assumptions and relations 11 through 13, the amount of $n^{ext}_{H_2O}$ and $n^{ext}_{CO_2}$ may readily be calculated. The results of these calculations indicate that 1000 cm^3 of sample JP9307 were infiltrated by 1.307 moles of CO$_2$ and 24.83 moles of H$_2$O. Converting from moles to

Tab. 9 Numbers of moles of CO_2 and H_2O, molar volume of mixed CO_2-H_2O fluid, and fluid flux values for four samples. Molar volumes of H_2O and CO_2 calculated for 520 °C and a pressure of 7 kbar using the equation of state for CO_2 and H_2O by KERRICK and JACOBS (1981) are $\overline{V}_{H_2O} = 20.27$ cm³/mol and $\overline{V}_{CO_2} = 38.03$ cm³/mol, respectively.

	[1] nCO_2	[2] nH_2O	[3] V_{fluid} cm³	[4] $V_{fluid flux}$ cm³
	1000 cm³	1000 cm³	1000 cm³	cm²
JP9307	1.307	24.83	553.01	55.30
PK9136	1.114	21.17	471.48	47.15
PK9191	3.741	71.08	1583.06	158.31
PK9149	2.399	45.58	1015.41	101.54

Explanations: **1** values from table 7; **2** values calculated from column 1 and relations 11 trough 13; **3** molar volume of mixed CO_2–H_2O fluid per liter of rock calculated from column **1, 2**, $\overline{V}_{H_2O} = 20.27$ cm³/mol, and $\overline{V}_{CO_2} = 38.03$ cm³/mol; **4** fluid flux through the first amphibolite layer with a thickness of 1 m.

volume using the data by KERRICK and JACOBS (1981), the total amount of fluid, which infiltrated one liter of sample JP9307 equals to 553 cm³. This results in a fluid/rock ratio (by volume) of about 55%. Fluid/rock ratio calculations for samples PK9136, PK9149, and PK9191 were performed according to the scheme outlined above assuming a value of 0.05 for $X_{CO_2}^{eq}$. The fluid/rock ratio derived from this procedure may also be converted to minimum estimates of fluid flux values in terms of volume fluid through a unit area of rock. Because the base of the amphibolite layers define a distinct interface in the fluid-rock system and have a thickness of 1 m, one may also argue that one cm² of this interface was infiltrated by appproximately 55 cm³ of fluid in the case of sample JP9307. Fluid flux values for the different samples are presented in table 9.

Discussion and conclusion

Compositional variations of calcic amphiboles from two samples indicate an increase in the ts, pl, and ed exchange components from the core of amphibole clasts to their rims and the matrix amphiboles. The rims of the amphibole clasts show compositional variations that are similar to those of the matrix amphiboles. This indicates that amphibole rims equilibrated during this stage of metamorphism. As shown by ROBINSON et al. (1982), the increase in the ts, pl, and ed exchange components in amphiboles is typically related to an increase of metamorphic conditions. According to PARTZSCH and MEYRE (1995), the progres-

sive metamorphic evolution recorded by these rocks occurred during the greenschist to epidote-amphibolite facies transition.

Overall mineral reactions were determined for two samples from the base of the Adula nappe. In absence of CO_2, progressive metamorphism of a protolith consisting of a combination of plagioclase low in anorthite component, calcic amphibole relatively poor in ts, pl, and ed components, biotite, and rutile produced an amphibole rich in ts, pl, and ed components, clinozoisite, and titanite or ilmenite. Rocks infiltrated by a mixed CO_2–H_2O fluid produced the same phases as above with additional calcite. The amount of biotite remained almost constant; plagioclase was consumed during the reaction. The remaining plagioclase changed its composition along the reverse pl exchange vector and thus became richer in Ca. Alterations such as those described in this study are common during the greenschist to epidote-amphibolite facies transition and during the epidote-amphibolite to amphibolite facies transition in mafic rocks (see ROBINSON et al., 1982).

Fluid flux calculations are generally performed in terms of fluid/rock ratios expressed as volume fluid per volume rock (compare FERRY 1984; RICE and FERRY, 1982). Fluid/rock ratios do not contain any information on the direction of the flow as opposed to fluid flux models such as provided by BAUMGARTNER and FERRY (1991) and FERRY and DIPPLE (1991). However, the fluid/rock ratio estimates presented in this study allow an estimation of the minimum fluid flux through a specific unit area of rock without appealing to infiltration of a fluid of unrealistic composition (e.g., FERRY, 1984). The direction of the fluid flow may be derived from field observations and petrologic data. As shown previously, CO_2 metasomatism was observed in amphibolites of both the Adula (PK9136, PK9191, and JP9307), and the Simano nappe (PK9149). The Adula nappe samples suggest the fluid flowed upward the rock column, whereas the Simano specimen indicates that the fluid flowed down the rock column. This suggests that the fluid was released from the metacarbonates from the Soja zone and entered the surrounding country rocks. During passage through the first amphibolite layer, all CO_2 in the fluid reacted with the rock. In other words, the first amphibolite layer acted as a filter that absorbed CO_2 from the infiltrating fluid. During the process of infiltration, the local mineral reactions proceeded by adjusting the compositions of the minerals and the mineralogy of the rock toward an equilibrium with the fluid. Field observations and petrologic data suggest that these processes occurred during progressive metamor-

phic evolution and emplacement of the Adula onto the Simano nappe and its autochthonous cover, the Soja zone (PARTZSCH and MEYRE, 1994; 1995; this study).

The importance of infiltration versus internal buffering was reviewed by RICE and FERRY (1982). A review of a representative set of studies led these authors to conclude that buffering is by far the more important mechanism. External control of the fluid composition was described by a few workers only (see references in RICE and FERRY, 1982). As previously mentioned, metamorphism driven by fluid infiltration requires different amounts of fluid fluxes. High fluxes on the order of 10^4–10^6 cm^3/cm^2 were assumed to be required for CO_2 metasomatism (e.g., carbonation or decarbonation reactions), whereas H_2O metasomatism (e.g., hydration or dehydration reactions) requires lower values on the order of 10^2–10^4 cm^3/cm^2 (FERRY and DIPPLE, 1991). On the other hand, in a previous paper, RICE and FERRY (1982) concluded that infiltration of large quantities of CO_2 were not reported to that date. We would like to emphazise that a shift of the invariant point in figure 7 (caused by varying activity values for the minerals) results in different $X^{eq}_{CO_2}$ values, and this in turn results in different estimates of fluid flux. However, our results indicate that the amount of fluid infiltration is relatively low, on the order of 57–158 cm^3/cm^2, and thus in agreement with RICE and FERRY (1982).

Acknowledgements

References

BAUMGARTNER, L.P. and FERRY, J.M. (1991): A model for coupled fluid flow and mixed volatile mineral reactions with applications to regional metamorphism. Contr. Mineral. Petrol., 106, 273–285.

BERMAN, R.G. (1988): Internally-consistant thermodynamic data for minerals in the system Na$_2$O–K$_2$O–CaO–MgO–FeO–Fe$_2$O$_3$–Al$_2$O$_3$–SiO$_2$–TiO$_2$–H$_2$O–CO$_2$. J. Petrol., 29, 445–522.

BROWN, T.H., BERMAN, R.G. and PERKINS, E.H. (1988): GE0-CALC: software package for calculation and display of pressure-temperature-composition phase diagrams using an IBM or compatible personal computer: Computers and Geosciences, 14, 279–298.

DALLA TORRE, M., DE CAPITANI, C., FREY, M., UNDERWOOD, M., MULLIS, J. and COX, R. (1996): Very low-grade metamorphism of shales from the Diablo Range, Franciscan Complex, California, USA: new constraints on the exhumation path. Bull. Geol. Soc. Am., in press.

DROOP, G.T.R. (1985): Alpine metamorphism in the south-east Tauern Window, Austria: 1. P-T variations in space and time. J. metam. Geol., 3, 371–402.

ENGI, M., TODD, T.S. and SCHMATZ, D.R. (1995): Tertiary metamorphic conditions in the eastern Lepontine Alps. Schweiz. Mineral. Petrogr. Mitt., 75, 347–369.

FERRY, J.M and DIPPLE, G.M (1991): Fluid flow, mineral reactions and metasomatism. Geology, 19, 211–214.

FERRY, J.M. (1984): A biotite isograd in South-Central Maine, U.S.A: mineral reactions, fluid transfer and heat transfer, J. Petrol., 25/4, 871–893.

FERRY, J.M. (1991): Dehydration and decarbonation reactions as a record of fluid infiltration. In: FERRY, J.M. (ed.): Rev. Mineral. Mineral. Soc., 26, 351–394.

FERRY, J.M. (1995): Fluid flow during contact metamorphism of ophicarbonate rocks in the Bergell aureole, Val Malenco, Italian Alps. J. Petrol., 36/4, 1039–1053.

FRANTZ, J.D. and WEISBROD, A. (1974): Infiltration metasomatism in the system K$_2$O–SiO$_2$–Al$_2$O$_3$–H$_2$O–HCl. In: HOFMANN, A.W., GILETTI, B.J., YODER, H.S. Jr., YUND, R.A. (eds): Geochemical transport and kinetics, Carnegie institution of Washington, 634, 261–271.

GREENWOOD, H.J. (1975): Buffering of pore fluids by metamorphic reactions. Am. J. Sci., 275, 573–593.

HEINRICH, C.A. (1986): Eclogite facies regional metamorphism of hydrous mafic rocks in the Central Alpine Adula nappe. J. Petrol, 27., 123–154.

HOLLAND, T.J.B. and POWELL, R. (1990): An enlarged and updated internally consisted thermodynamic dataset with uncertainties and correlations: the system K$_2$O–Na$_2$O–CaO–MgO–MnO–FeO–Fe$_2$O$_3$–Al$_2$O$_3$–TiO$_2$–SiO$_2$–H$_2$O–C–H$_2$–O$_2$. J. metam. Geol., 8, 89–124.

KERRICK, D.M. and JACOBS, G.K. (1981): A modified Redlich-Kwong equation for H$_2$O, CO$_2$ and H$_2$O–CO$_2$ mixtures at elevated pressures and temperatures. Am., J. Sci., 281, 735–767.

KORZHINSKII, D.S. (1970): Theory of metasomatic zoning, Clarendon press, Oxford, 1–74.

KRUSPAN, P. (1993): Petrographische und strukturgeologische Untersuchungen im Grenzbereich der Adula- und Simano-Decke südwestlich des Rheinwaldhorns (Val Malvaglia, TI). Unpub. Diploma thesis, Basel.

KUNIYOSHI, S. and LIOU, J.G. (1976): Contact metamorphism of the Karmutsen Volcanics, Vancouver, Island, British Columbia. J. Petrol., 17., 73–99.

LÉGER, A. and FERRY, J.M. (1993): Fluid infiltration and regional metamorphism of the Waits River Formation, north-east Vermont, USA. J. metam. Geol., 11, 3–29.

PARTZSCH, J.H., DALLA TORRE, M., FREY, M., MEYRE, C. and DE CAPITANI, C. (in prep.): The metamorphic evolution of the Adula nappe, Central Alps, Switzerland.

PARTZSCH, J.H. and MEYRE, C. (1994): Die tektonometamorphe Entwicklung der mittleren Adula-Decke (Zentralalpen, Schweiz). Göttinger Arb. Geol. Paläont. Sb 1, 5. Symposium TSK, Göttingen, 124–126.

PARTZSCH, J.H. and MEYRE, C. (1995): The structural evolution of the middle Adula nappe (Central Alps,

Switzerland). Bochumer geol. geotech. Arb., 44, Abstract volume: Internat. Colloquium, 136–138.

RASBAND, Z. (1993): IMAGE Version, 1.52, public domain program.

RICE, J.M. and FERRY, J.M (1982): Buffering, infiltration and the control of intensive variables during metamorphism. In: Rev. Mineral. Ed. KERRICK, D.M., Mineral. Soc., 10, 263–326.

ROBINSON, P., SPEAR, F.S., SCHUMACHER, J.C., LAIRD, J., KLEIN, C., EVANS, B.W. and DOOLAN, M.C. (1982): Phase relations of metamorphic amphiboles: natural occurrence and theory. In: VEBLEN, D.R. and RIBBE, P.H. (eds): Rev. Mineral., Mineral. Soc., 9b, 1–228.

SCHMID, S., FROITZHEIM, N., PFIFFNER, A., SCHOENBORN, G. and KISSLING, E. (1996): Geophysical-geological transect and tectonic evolution of the Swiss-Italian Alps. Tectonics, in press.

SCHMID, S., RÜCK, P. and SCHREURS, G. (1990): The significance of the Schams nappes for the reconstruction of the paleotectonic and orogenic evolution of the Pennin zone along the NFP-20 East traverse (Grison, eastern Switzerland). In: ROURE, F., HEITZMANN, P. and POLINO, R. (eds): The deep structure of the Alps. Mém. Soc. géol. Fr., Paris, 156, 263–288.

SPEAR, F.S. (1993): Activity models for phases of petrologic importance. In: SPEAR, F.S. (ed.): Metamorphic phase equilibria and pressure-temperature-time paths. Min. Soc. Am. Monograph.

STOUT, J.H. (1972): Phase petrology and mineral chemistry of coexisting amphiboles from Telemark, Norway. J. Petrol, 13, 99–146.

THOMPSON, J.B. Jr. (1982a): Composition space: an algebraic approach. In: FERRY, J.M. (ed.): Rev. Mineral. Mineral. Soc., 10, 1–32.

THOMPSON, J.B. Jr. (1982b): Reaction space: an algebraic approach. In: FERRY, J.M. (ed.): Rev. Mineral. Mineral. Soc., 10, 33–52.

THOMPSON, J.B. Jr., LAIRD, J. and THOMPSON, A.B. (1982): Reactions, in amphibolite, greenschist and blueschist. J. Petrol, 23, 1–27.

WOOD, J.B. and WALTHER, J.V. (1986): Fluid-flow during metamorphism and its implications for fluid-rock ratios. In: WALTHER, J.V., WOOD, J.B. (eds): Fluid-rock interactions during metamorphism. Springer Verlag, New York, 89–108.